Review of Scientific Instruments

A hot-film air flow sensor for elevated temperatures

Cite as: Rev. Sci. Instrum. **90**, 015007 (2019); https://doi.org/10.1063/1.5065420
Submitted: 09 October 2018 . Accepted: 07 January 2019 . Published Online: 28 January 2019

Vivekananthan Balakrishnan, Toan Dinh, Thanh Nguyen, Hoang-Phuong Phan, Tuan-Khoa Nguyen, Dzung Viet Dao, and Nam-Trung Nguyen

AIP Publishing

Review of Scientific Instruments | ARTICLE | scitation.org/journal/rsi

A hot-film air flow sensor for elevated temperatures

Cite as: Rev. Sci. Instrum. 90, 015007 (2019); doi: 10.1063/1.5065420
Submitted: 9 October 2018 • Accepted: 7 January 2019 •
Published Online: 28 January 2019

View Online | Export Citation | CrossMark

Vivekananthan Balakrishnan,[1] Toan Dinh,[1] Thanh Nguyen,[1] Hoang-Phuong Phan,[1] Tuan-Khoa Nguyen,[1] Dzung Viet Dao,[1,2] and Nam-Trung Nguyen[1,a)]

AFFILIATIONS

[1] Queensland Micro-Nanotechnology Centre, Griffith University, Brisbane, QLD 4111, Australia
[2] School of Engineering, Griffith University, Gold Coast, QLD 4222, Australia

[a)] Author to whom correspondence should be addressed: nam-trung.nguyen@griffith.edu.au

ABSTRACT

We report a novel packaging and experimental technique for characterizing thermal flow sensors at high temperatures. This paper first reports the fabrication of 3C-SiC (silicon carbide) on a glass substrate via anodic bonding, followed by the investigation of thermoresistive and Joule heating effects in the 3C-SiC nano-thin film heater. The high thermal coefficient of resistance of approximately −20 720 ppm/K at ambient temperature and −9287 ppm/K at 200 °C suggests the potential use of silicon carbide for thermal sensing applications in harsh environments. During the Joule heating test, a high-temperature epoxy and a brass metal sheet were utilized to establish the electric conduction between the metal electrodes and SiC heater inside a temperature oven. In addition, the metal wires from the sensor to the external circuitry were protected by a fiberglass insulating sheath to avoid short circuit. The Joule heating test ensured the stability of mechanical and Ohmic contacts at elevated temperatures. Using a hot-wire anemometer as a reference flow sensor, calibration tests were performed at 25 °C, 35 °C, and 45 °C. Then, the SiC hot-film sensor was characterized for a range of low air flow velocity, indicating a sensitivity of 5 mm^{-1} s. The air flow was established by driving a metal propeller connected to a DC motor and controlled by a microcontroller. The materials, metallization, and interconnects used in our flow sensor were robust and survived temperatures of around 200 °C.

I. INTRODUCTION

Sensors for the harsh environment include but are not limited to the detection of pressure,[1,2] strain,[3–5] temperature,[6] flow,[7,8] acceleration,[9,10] and others.[11,12] An environment is considered as harsh with high temperature (≫400 K), cryogenic temperature (<273 K), high pressure (≫0.1 MPa) or vacuum, chemically reacting and oxidising fluids, electromagnetic and nuclear radiation.[13] These conditions require robust and stable materials for various sensing applications. For instance, aluminium nitride, lithium niobate, lead zirconate titanate have been commonly utilized for piezoelectric and ultrasonic sensing applications.[14–16] On the other hand, platinum,[17] diamond,[18] low-temperature co-fired ceramics (LTCC),[19] stainless steel,[20] yttria-zirconia,[21] and silicon compatible materials[22,23] have been used for temperature and flow sensing applications. The application areas with these environments include aerospace,[24] automotive,[25] industrial process control,[26] and sea exploration.[27] For instance, measuring flow velocity and flow rate in harsh environments is critically important in the automotive industry because of the presence of high temperature, corrosives, and particulates. For instance, accurate air flow control in the fuel injection system can provide a better performance of internal combustion engine, increase fuel efficiency, and reasonably reduce emissions.[28] Therefore, precise and continuous monitoring of fluid flow is important and thus requires highly stable solid-state sensors and electronics.

The commonly employed instruments for flow measurement in the harsh environment include an ultrasonic flow meter,[29] a vane wheel flow meter,[30] and a vortex flow meter.[31]

These flow meters suffer from large size, high power consumption, low response time, and high cost. To resolve these limitations, microelectromechanical systems (MEMSs)-based flow sensors such as thin film mass air flow (MAF) sensor[32] and micro-bridge flow sensor[33] have been utilized for various applications. Moreover, advances in MEMS technology led to the development of high-performance and sensitive micromachined flow sensors over the past few years.[1] In general, MEMS flow sensors can be categorized into two groups: thermal and non-thermal flow sensors. Due to the robust stationary parts and electronic simplicity, thermal flow sensors are more often employed for flow sensing than their counterparts.

Thermal flow sensors operate based on Joule heating and are classified into three configurations: hot wire/hot film, calorimetric, and time of flight.[34] Hot-wire/hot-film thermal flow sensors sense the cooling effect of fluid flow via convective heat transfer from an electrically heated sensing element.[35,36] Calorimetric thermal flow sensors measure the asymmetry of the temperature distribution around the heating element using an upstream and a downstream temperature sensor.[37] Time of flight sensors measure the delay from the injection of heat pulse from a heater to the detection of the pulse by the temperature sensor.[38,39]

According to the physical transduction mechanism, thermal flow sensors are categorized as thermoresistive, thermoelectric, and thermoelectronic.[40] Thermoresistive sensors employ resistive elements such as thermistors, resistance-temperature detectors (RTDs) for temperature sensing. Thermoelectric sensors are based on the conversion of temperature difference into a voltage by a thermocouple. In the case of thermoelectronic sensors, diodes, bipolar junction transistors (BJTs), and field effect transistors (FETs) are commonly utilized for temperature sensing.[41] In recent years, numerous works on thermoresistive hot-wire,[42–44] hot-film,[45–47] and calorimetric air flow sensors[17,48,49] have been reported in the literature. Nevertheless, the design and characterization of thermoresistive air flow sensors for high-temperature applications (higher than 150 °C) have been rarely reported.

The most important consideration for the development of a thermal flow sensor is the material choice. Heating/sensing materials can be made of metals and semiconductors. Metals can be deposited as a thin film on a chip to realise the heating element. The commonly employed metals include nichrome,[50] platinum,[51] and tungsten.[52] Although these materials are mechanically strong and possess linear thermoresistive response, the thermal sensitivity as quantified by the temperature coefficient of resistance (TCR) is relatively low, on the order of few thousand ppm/K.[53]

On the other hand, micromachining techniques have enabled the production of silicon-,[54] germanium-,[55,56] polysilicon-,[57] graphite-,[58] and carbon nanotubes (CNTs)[59]-based thermal sensors for flow measurement. These semiconductors exhibit a wide range of TCR values from positive to high negative and can also be tuned using different doping levels or changing growth parameters.[60,61] However, the thermoresistive properties of silicon, germanium, and polysilicon impose limitations on the use at high operating temperatures and harsh media. Other materials such as graphite and CNTs exhibit non-linearity and hysteresis and possess large resistivity; hence, they are not suitable for thermal flow sensor applications, which involve heating elements. In addition, the current difficulties in releasing these materials challenge the use in Joule heating-based thermal sensors. To overcome these drawbacks, an alternative material that offers high thermoresistive sensitivity, compatible with MEMS fabrication techniques, and also the ability to work under harsh environments needs to be identified.

Silicon carbide (SiC), an alternative semiconductor material, has gained a reputation for its promising application in harsh environments owing to the wide bandgap, mechanical stability, and high melting point. Among the various polymorphic structures of SiC, 3C, 4H, and 6H crystals were identified and employed to date for various sensing applications.[62] Compared with 4H and 6H-SiC, 3C-SiC can be epitaxially grown on a readily available silicon substrate at a low cost. Moreover, the lower growth temperature of 3C-SiC makes it the more favourable material for many MEMS applications than 4H and 6H polytypes. Due to the recent developments in processing techniques and controlled material properties, a number of 3C-SiC MEMS sensors were widely reported in the literature.[63–65] For instance, we reported for the detailed fabrication and testing of thermal air flow sensor based on SiC technology. Moreover, a detailed investigation of the thermoresistive properties of 3C-SiC led to the flow measurements. The relationship between the geometry of the SiC heater and sensor performance was also studied along with the effect of flow direction. The main purpose of this work was the development

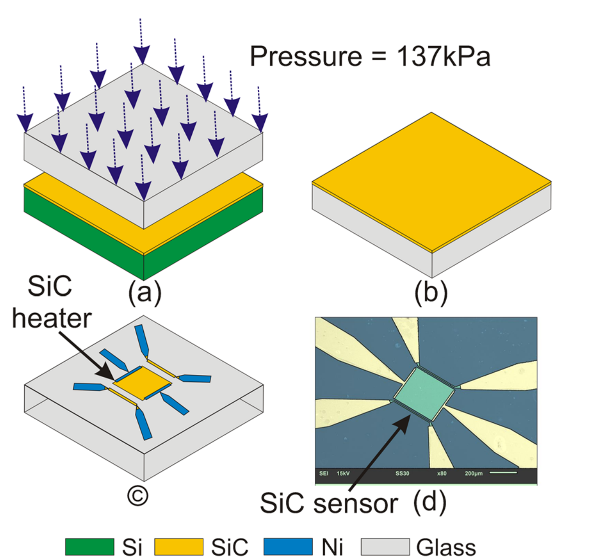

FIG. 1. Fabrication of the SiC temperature sensors and heaters on a glass substrate: (a) Bonding of SiC/Si on the glass; (b) Removal of Si to form SiC on the glass; (c) SiC thermal flow sensor after photoresist (PR) coating, patterning, etching, and nickel deposition; and (d) Scanning Electron Microscope (SEM) image of the fabricated thermal flow sensor (false color).

of a highly sensitive flow sensor at room temperatures.[66] The successful test at room temperature motivated us to develop SiC flow sensors for elevated temperatures.

For the sensor to survive the high temperature, we propose a novel packaging technique to suitably characterize the flow sensor at temperatures up to 200 °C. Various challenging aspects in this work have been addressed in the context of harsh environments: material choice, metallization interconnects, Ohmic contact stability, measurement setup, and flow calibration.

II. DEVICE FABRICATION

Figure 1 illustrates the fabrication process of the 3C-SiC thermal flow sensor. The 3C-SiC wafer was provided by the Queensland Microtechnology Facility (QMF) at Griffith University, Australia. Initially, single crystalline cubic silicon carbide films were epitaxially grown on a 6-in. silicon (111) substrate. The growth process was performed with low-pressure chemical vapour deposition (LPCVD), where silane and propylene were employed as silicon- and carbon-containing sources. The growth process was followed by a plasma-enhanced anodic bonding, where the SiC/Si was bonded to a glass wafer (Boroflat 33, University Wafers, South Boston, United States) at a maximum pressure of 137 kPa and a bias voltage of 1000 V, Fig. 1(a).

The anodic bonding process was followed by mechanical polishing and wet etching processes using a mixture of HF, HNO_3, and CH_3COOH with a ratio of 2:2:3 to form SiC on a glass substrate, Fig. 1(b). Subsequent processes of photoresist (PR) coating, photolithography, and patterning of SiC layers were performed prior to nickel (Ni) deposition. Then, the Ni electrodes were patterned using standard photolithography and wet etching processes, Fig. 1(c). Figure 1(d) depicts the SEM image of the fabricated SiC sensor on the glass substrate (false coloured image). The SiC heater measures 1000 μm × 1000 μm × 300 nm, and the sheet resistance ($R_s = \rho/t$) and the electrical resistivity were determined as 258 kΩ/sq. and 7.74 Ωcm, respectively. The detailed fabrication process has been reported recently and can be found elsewhere.[66]

III. MEASUREMENT SETUP

Figure 2 shows the prepared device and various components employed for the characterization setup of the flow sensor. Initially, the thermal sensor was affixed to a glass slide using a high-temperature epoxy that could withstand

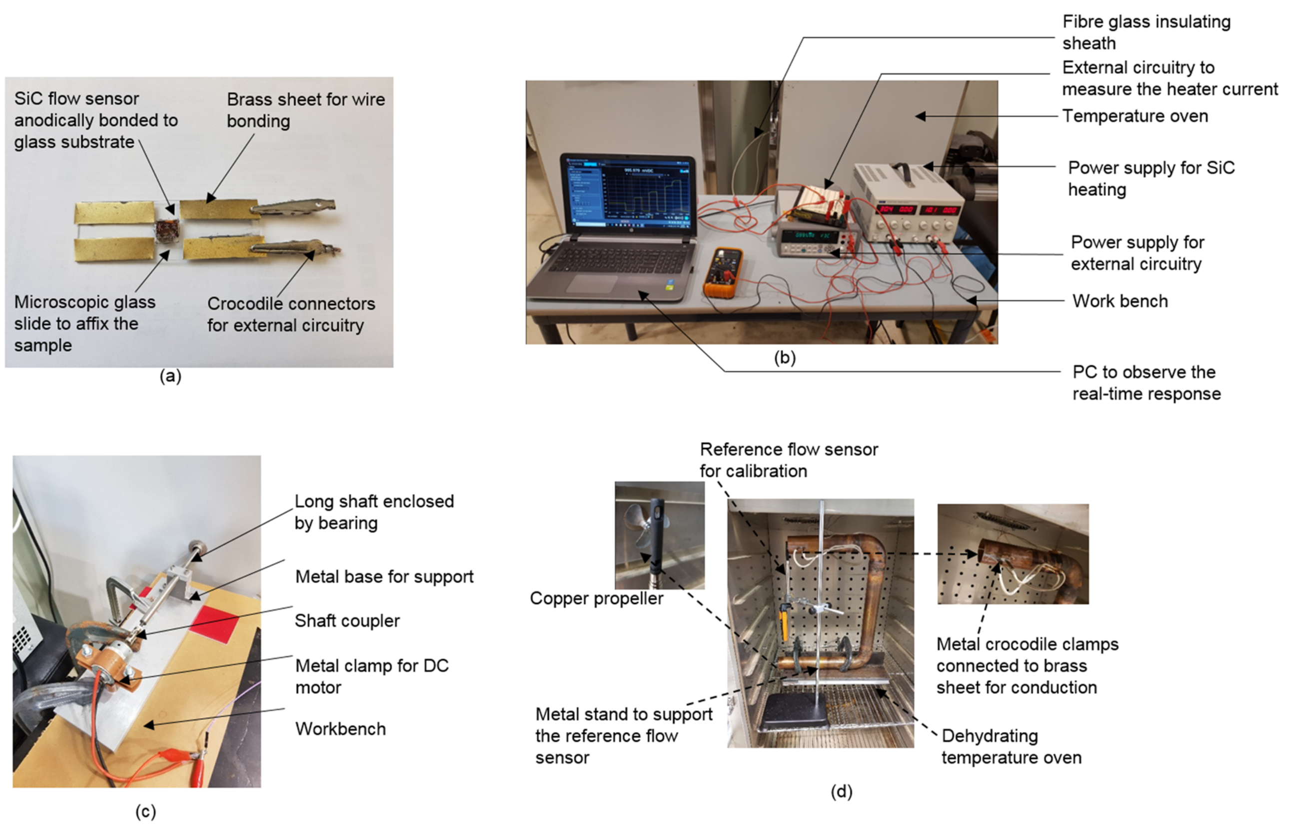

FIG. 2. Measurement setup for elevated temperature conditions: (a) Preparation of high-temperature interconnects; (b) Joule heating setup at elevated temperatures; (c) DC motor control setup for flow measurement; and (d) Flow calibration setup incorporating copper flow channel.

temperatures up to 260 °C. Then, brass sheets were suitably cut and attached to the glass substrate using the epoxy for wire bonding as shown in Fig. 2(a).

Figure 2(b) depicts the Joule heating measurement and data logging setup. The sensor was fixed on a metal slab and placed inside a dehydrating temperature oven (TD 500-F) for characterization. The interconnects from the sensor to the external measurement circuit were established by using a metallic crocodile connector enclosed by a fiberglass insulating sheath. Through an electrical inlet, a K-type thermocouple wire was fixed near the sensor chip to monitor the actual temperature. Then, the real-time data were logged with the help of a computer.

A 9 V DC motor coupled to a 38-cm-long shaft was utilized to drive a copper propeller for generating air flow. The motor speed was controlled by an Arduino Uno microcontroller board. Figure 2(c) shows the motor setup, where the shaft runs into the electrical inlet of the temperature oven. Enough clearance was obtained between the shaft and electrical inlet to avoid friction.

The flow channel was level adjusted to the position in front of the propeller, and a hot-wire anemometer (Testo450i wireless smart probe) was used as a reference flow sensor. Figure 2(d) shows the measurement setup with flow sensing capability at elevated temperatures. A copper pipe with a length of 1 m and an inner diameter of 5 cm was employed as a flow channel. The long pipe was precisely cut and welded to two suitable 90° elbow radius pipes to obtain a U-shaped design. Two mechanical clamps and a slab were utilized to support the flow channel. In addition, a fiberglass insulating sheath and a metal wire were employed to establish the interconnects with the instruments outside the oven. On the other end of the channel, a slit was created to insert the sensor chip, and the epoxy was used for strong attachment.

Once the initial setup was made, the reference flow sensor was placed near the device and the flow velocity was monitored by a Bluetooth-based controller. The oven was turned on for flow calibration at temperatures of 25 °C, 35 °C, and 45 °C, respectively. The actual temperature and warm-up time were monitored by a K-type thermocouple and a stop clock, respectively. Using the microcontroller Arduino Uno, a series of air flow velocities was set at the above three temperatures. A repeatability test was carried out to ensure the accuracy of the calibration. Moreover, the calibration at these temperatures indicated good repeatability of air flow velocity and was used subsequently for flow characterization.

IV. RESULTS AND DISCUSSIONS

A. Thermoresistive effect

In a single crystalline n-type 3C-SiC heating film, the number of free charge carriers increases with increasing temperature due to thermal energy excitation. On the other hand, the mobility of SiC film decreases with increasing temperature due to the scattering effect of lattice vibrations.[67]

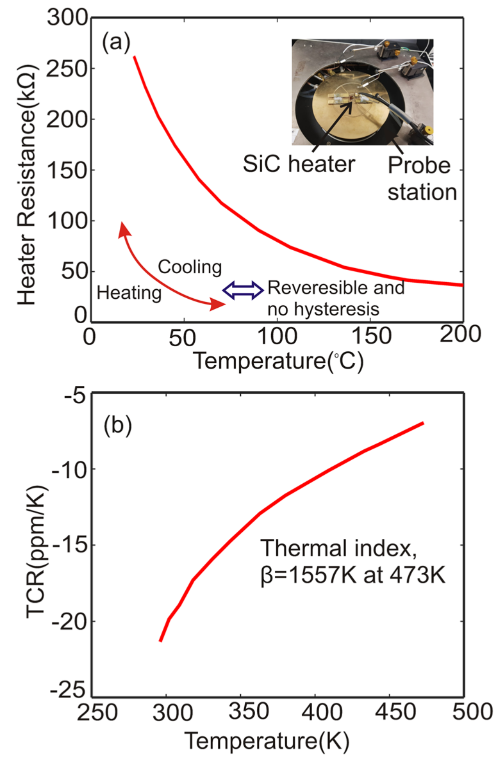

FIG. 3. Characterization of the SiC heater at elevated temperatures: (a) Thermoresistive characteristics. The inset shows the measurement setup. (b) Temperature coefficient of resistance (TCR) characteristics.

This leads to a decrease in the electrical resistance and the resistivity of the film. Figure 3(a) depicts the variation in heater resistance with temperature, and the inset illustrates the measurement setup for investigating the thermoresistive effect. Before conducting the electrical and flow measurements, the SiC heater was characterized with this setup. The nano-thin film was placed on a probe station and positioned precisely with a thin needle for recording electrical resistance during the heating phase. With an equal interval of 20 °C, the resistance of the heater was measured using an ohmmeter (QM 1535).

Figure 3(a) indicates that the relative change in resistance from the ambient temperature to 200 °C is about 80%. During the cooling phase, the resistance of the heater returned to its original value, thereby demonstrating good reversible characteristics with no hysteresis effect. The thermal coefficient of resistance (TCR) of the 3C-SiC film was calculated to range from −9286 ppm/K (473 K) to −20 730 ppm/K (298 K), which is reasonably higher than the TCR of materials previously reported in the literature.[68–70] This high TCR shown in Fig. 3(b) demonstrates the prospective of SiC film for developing sensitive thermal flow sensors. The detailed charge transport and activation energy mechanisms of 3C-SiC thin films have been reported in Ref. 71.

B. Ohmic contact and metallization stability test

Electrical measurements were performed under elevated temperature conditions. The I-V characteristics of the SiC heater at various operating temperatures are presented in Fig. 4(a). As the applied voltage increases, the heater current also increases linearly at low supply voltages to approximately 15-20 V and then follows the non-linear characteristics. The linear characteristics of the SiC indicate that the electrical resistance follows Ohm's law R = V/I. It is also important to note that the resistance is low at higher temperatures during Joule heating. For instance, the red curve (100 °C) shows highly resistive characteristics at approximately 20 V and the green curve (200 °C) is less resistive at the same supply voltage. When the ambient temperature increases, the ionization effect raises the carrier concentration and the electrical conductance.

This test suggests a low resistance and a stable Ohmic contact between the metal electrodes and SiC heater at all three different temperatures, respectively. Using a digital multimeter (DMM 34450A), the real-time heater current recorded for five different steps of supply voltage at 200 °C is shown in Fig. 4(b). In addition, the electrical characteristic of the SiC on a glass platform was found to be reversible for 4 cycles during simultaneous heating and cooling (not shown here).

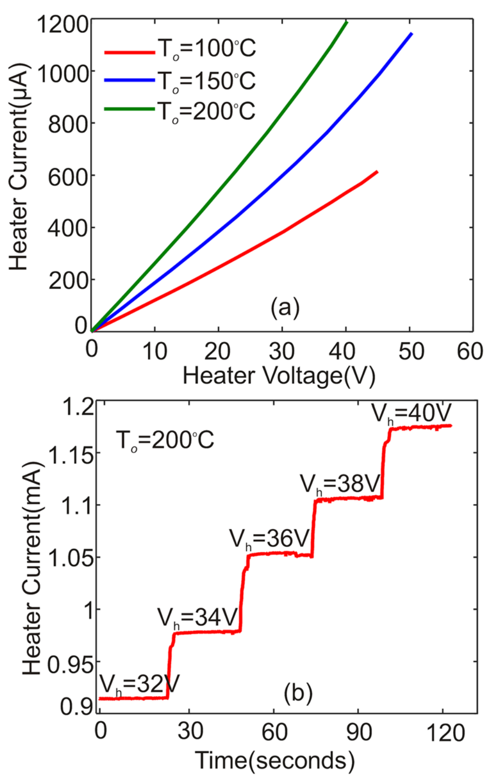

FIG. 4. Electrical characteristics of the SiC heater at elevated temperatures: (a) I-V curve at three different temperatures and (b) Real-time response at five different voltage steps.

The repeatability of our measurement indicates the strong metallization and interconnects from the heater to the external circuitry. Moreover, an Ohmic contact of low resistivity with long-term stability in harsh environments indicates the potential of SiC MEMS technology for various practical applications.

C. Joule heating effect

We also conducted the Joule heating experiment to study the relationship between the heater resistance and applied bias that will aid in the fluid flow characterization subsequently. Joule heat in the heater film generated by DC power is dissipated in three ways: conduction, convection, and radiation.[72] The radiation heat transfer could be ignored as the maximum operating temperature is 200 °C. The main energy loss due to conduction occurs from SiC heating film to Ni electrodes and from the film to the glass substrate. However, the heat loss due to conduction is small because of the low thermal conductivity of the glass substrate.

Under non-flow conditions, the non-linear characteristics (R_h-V_h characteristic) shown in Figs. 5(a)–5(c) reflect the change in heater temperature and heater resistance with the supplied bias at different oven temperatures. The relative change in heater resistance can be calculated as

$$\Delta R_h / R_h = \frac{R_{heatingon} - R_{heatingoff}}{R_{heatingoff}}, \tag{1}$$

where $R_{heatingon}$ and $R_{heatingoff}$ represent the initial resistance prior to supplying the bias and the resistance of a stable data shown on the ohmmeter after providing the bias, respectively. A simple series electrical circuit was designed to measure the voltage drop across the external resistor, R_{ext}, and thereby, R_h was calculated [inset of Fig. 5(a)]. Using Eq. (1), the relative resistance change accounts for 4.88%, 2.72%, and 1.75% for ambient temperatures of 100 °C, 150 °C, and 200 °C, respectively, Fig. 5(d). The heating power could be estimated as follows: $P_h = V_h^2/R_h$, where V_h and R_h are the voltage applied on the heater and heater resistance, respectively. It is notable that due to reduced heat loss into the glass substrate, only a magnitude of milliwatt heating power is needed to observe a significant change in heater resistance. The low-power operation of our SiC heating film strongly reveals the potential for sensitive thermal flow sensors working at elevated temperatures.

D. High-temperature flow testing

The fabricated thermal flow sensor in Fig. 1(d) represents the calorimetric configuration composed of a central heater and an upstream and downstream temperature sensor. However, we utilized only the heating element for high-temperature flow testing. The inset in Fig. 6(a) shows the working principle of the hot-film flow sensor inside an oven. As such, when a large bias is applied to the heater, a temperature rise occurs around the SiC film due to the Ohmic loss and reaches a steady state when the heat loss is equal to

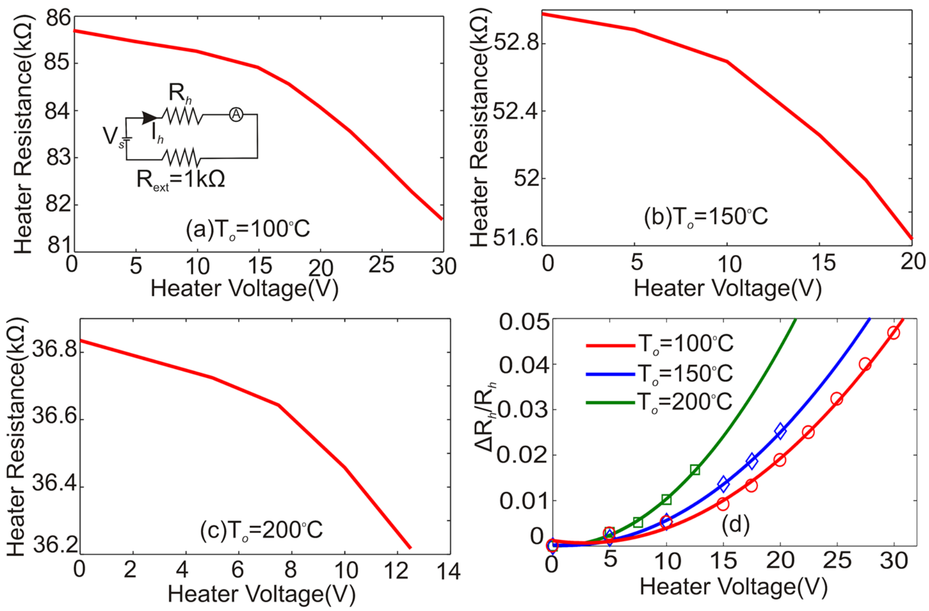

FIG. 5. Characterization of the SiC hot-film sensor at elevated temperatures using Joule heating effect: (a) T_o = 100 °C. The inset shows an external electrical circuit to measure the voltage drop across the external resistor, R_{ext}. (b) T_o = 150 °C. (c) T_o = 200 °C. (d) Normalized heater resistance versus heating voltage.

the supplied power.[73] At the steady state, the following equation describes the relationship between the heating power and convective heat loss under the constant voltage mode (V_h = constant):

$$\frac{{V_h}^2}{R_h} = hA(T - T_f), \tag{2}$$

where R_h, A, and T are the heater resistance, surface area of the film, and heater temperature, respectively; T_f is the temperature of the fluid (air); and h is the convective heat transfer coefficient. The steady-state output of a hot film should follow King's law, which states that

$$h = a + bV_f^n, \tag{3}$$

where a, b, and n are constants and V_f is the air velocity. The temperature and resistance of the heating film exposed to the air flow could be measured easily if the TCR is higher for the material and vice versa.[74] For instance, the thermal sensors proposed in Refs. 75 and 76 provide low thermoresistive sensitivity and so sensing temperature changes is challenging. Consequently, the resistance change ($\Delta R_h/R_h$) is generally converted into voltage (ΔV_h) change by a Wheatstone bridge circuit and amplified later to observe the sensor response. Nevertheless, the high TCR of our SiC heating film shown in Figs. 3(b) and 6(b) strongly suggests that the resistance change (%) could be easily observed during flow measurement. Accordingly, we have measured the heater resistance directly via ohmmeter, and the characteristics are shown in Figs. 6(c)–6(e).

When an air flow passes around the film, the power loss increases and the temperature of the heater film decreases. This leads to a increase in electrical resistance of the film, owing to the negative temperature coefficient of resistance (NTC) behavior. Figures 6(c)–6(e) show the resistance change in the heater with respect to the supplied voltage at three different ambient temperatures. It is noteworthy that the sensitivity due to air flow is higher at 100 °C and decreases with the rise in temperature. This is due to the reason that the steep temperature sensitivity curve of 3C-SiC becomes flat at higher temperatures as observed in Fig. 6(b). In other words, the absolute thermal coefficient of resistance decreases with increasing temperature. As a result, the R_h-V_f characteristics are observed to be non-linear at 100 °C and become linear with increasing temperature. We have also observed that the amount of change in resistance increases with the rise in supply voltage for the flow range. For instance, the resistance increases by 42% from 20 V to 30 V heating, as observed in Fig. 6(c). The data shown in Figs. 6(c)–6(e) were fitted by a quadratic polynomial. The R-squared value of quadratic fitting in Fig. 6(a) (heating voltage = 20 V) is equal to 0.98 implying the fit explains 98% of the total variation in the data about the average.

Figures 7(a)–7(c) show the variation in relative resistance change versus flow velocity for three different ambient temperatures. The slope of the relative change in resistance and flow velocity can be quantified by a parameter called flow sensitivity. It can be represented mathematically as follows:

$$S = \left(\frac{\Delta R_h/R_h}{V_f}\right) = \left(\frac{\frac{R_{flowon} - R_{flowoff}}{R_{flowoff}}}{V_f}\right), \tag{4}$$

where V_f represents the flow velocity in m/s. Using Eq. (4), the sensitivity due to the flow was calculated to be 5 mm^{-1} s at 100 °C, which reduces to 1.28 mm^{-1} s at 200 °C for a constant flow velocity of 1.29 m/s, Fig. 7(c). Also, the sensitivity increases with the supply voltage at all ambient temperatures, Fig. 7(b). For instance, the sensitivity for V_h = 27.5 V was estimated to be 3.87 mm^{-1} s, whereas it increases to 5 mm^{-1} s for V_h = 30 V, as shown in Fig. 7(a).

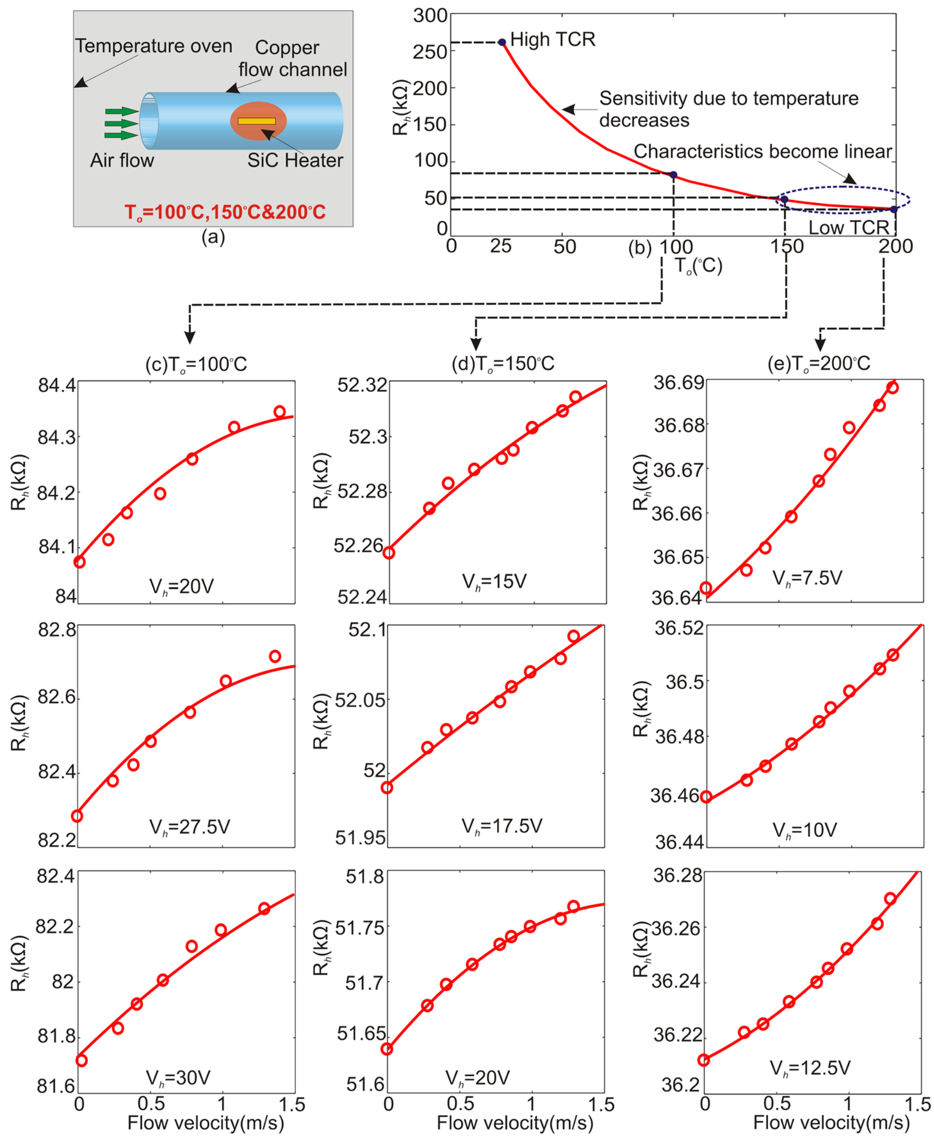

FIG. 6. Flow sensor characterization: (a) Operating principle; (b) Resistance-Temperature dependency; (c) T_o = 100 °C; (d) T_o = 150 °C; and (e) T_o = 200 °C.

We also observed that a higher flow velocity led to an increasing heater resistance due to cooling through forced convection. Figures 8(a)–8(c) illustrate the effect of air flow velocity due to Joule heating at three elevated temperatures. The heating voltages were different for the operating temperature. For instance, we limited the V_h to 30 V, 20 V, and 12.5 V at 100 °C, 150 °C, and 200 °C as a significant change in resistance was observed, as shown in Figs. 5(a)–5(c), and also for the safe operation of the device. It is evident that a resistance shift was observed from Figs. 8(a)–8(c) compared with Figs. 5(a)–5(c) due to the cooling effect. As the heating voltage is dependent on the air flow velocity, conduction heat loss will be dominant if the heating voltage is higher than the cooling rate. On the other hand, higher convective cooling can be obtained with the rise in flow velocities.

The regime of the flow can be quantified by an important parameter called Reynolds number. For flow in a pipe, the Reynolds number can be expressed as

$$Re_D = DV_f/\upsilon, \tag{5}$$

where D is the hydraulic diameter of the pipe, which is 0.05 m; V_f is the air flow velocity (m/s); and υ is the kinematic viscosity of air, which is 15.11 × 10^{-6} m^2/s. Laminar flow in a pipe occurs up to a Reynolds number of 2100, and transitional flow occurs between 2100 < Re_D < 4000. For Re_D > 4000, turbulent flow occurs. According to Eq. (5), the threshold velocity where the laminar flow

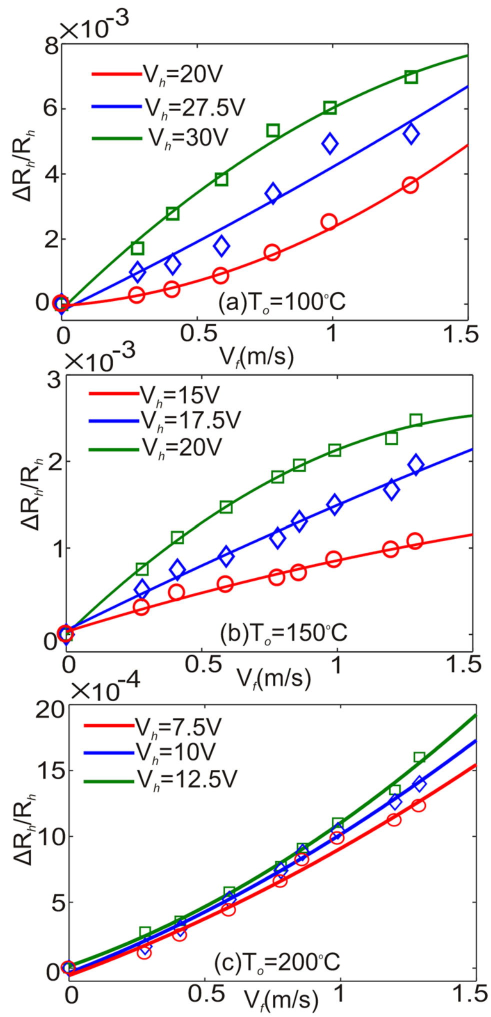

FIG. 7. Normalized flow response data for three different supply voltages: (a) T_o = 100 °C; (b) T_o = 150 °C; and (c) T_o = 200 °C.

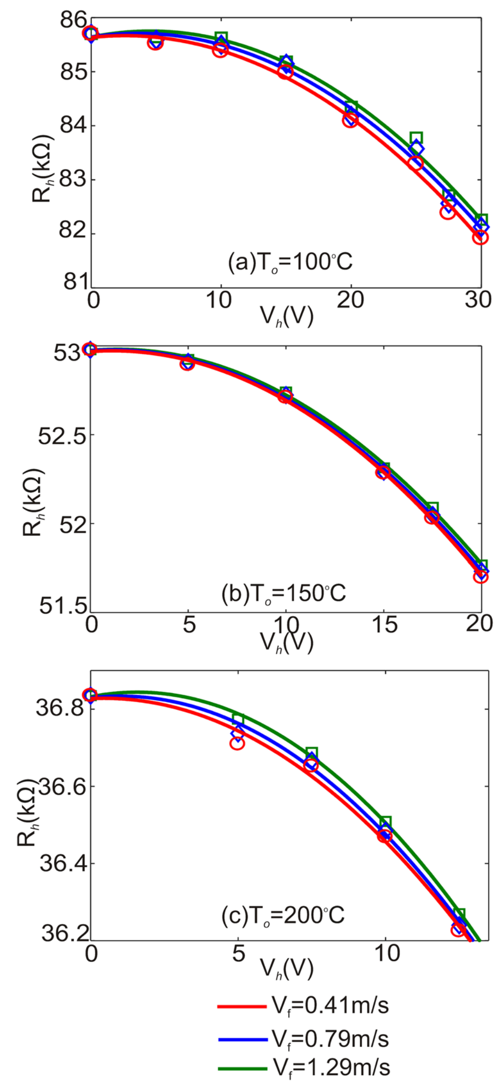

FIG. 8. Effect of the air flow velocity on the sensor output: (a) T_o = 100 °C; (b) T_o = 150 °C; and (c) T_o = 200 °C.

regime ends is 0.64 m/s and the transitional flow prevail between 0.64 < V_f < 1.23. The Re_D is estimated to range approximately from 330 to 4268 for the flow range of 0.1–1.29 m/s.

The maximum detectable air flow velocity in a high-temperature measurement setup could be very challenging. Our experimental setup depends on various constraints: (i) the outer diameter of the propeller and the number of blades, (ii) the hydraulic diameter of the copper pipe, (iii) the operating voltage of the dc motor employed, (iv) the size of the temperature oven, and (v) the size of the sensor chip. Due to the aforementioned factors, the maximum air flow velocity generated by our setup was 1.29 m/s.

Using the raw data presented in Fig. 8, the normalized change in heater resistance was plotted for a constant air velocity in Fig. 9. We observed that the heating voltage must

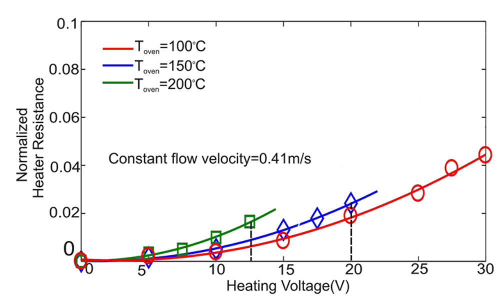

FIG. 9. Effect of the operating temperature on the heater output for a constant air flow velocity.

be high for lower temperatures to compensate the convective heat lost through the air flow. For instance, we applied a maximum of 12.5 V at 100 °C and 30 V at 200 °C to compensate for the heat loss for a constant flow velocity of 0.41 m/s. Consequently, the normalized heater output was found to be maximum at 100 °C and minimum at 200 °C.

V. CONCLUSIONS AND FUTURE OUTLOOK

We briefly reviewed the current state of art sensing materials and thermoresistive air flow sensing techniques for harsh environments and proposed a novel method to characterize thermal sensors in both the presence and absence of air flow at temperatures of around 200 °C. The SiC sensor fabricated using MEMS anodic bonding technique was packaged suitably to withstand high-temperature operation. Challenges encountered in the mechanical, electrical, and control parts of the measurement system were addressed accordingly. The results presented herein demonstrate that the sensor responds well to air flow up to approximately 1.5 m/s and requires only several milliwatts to operate. The sensor combines the advantages of small size, low power consumption, and high thermal sensitivity coupled with high temperature stability. However, the sensitivity of the flow sensor could be improved further with a calorimetric operation, which is highly sensitive to low flow velocities. Future works will also involve the design of free-standing structures, which will increase the sensor response time, an important characteristic of the thermal flow sensor.

ACKNOWLEDGMENTS

This work was performed in part at the Queensland Node of the Australian National Fabrication Facility, a company established under the National Collaborative Research Infrastructure Strategy to provide nano- and microfabrication facilities for Australia's researchers. The authors acknowledge funding support from the Australian Research Council through the ARC linkage Grant (No. LP150100153).

REFERENCES

[1]R. S. Okojie, A. A. Ned, and A. D. Kurtz, Sens. Actuators, A **66**, 200 (1998).

[2]R. Ziermann, J. von Berg, W. Reichert, E. Obermeier, M. Eickhoff, and G. Krotz, in 1997 *International Conference on Solid-State Sensors and Actuators, TRANSDUCERS'97, Chicago* (IEEE, 1997), pp. 1411–1414.

[3]R. G. Azevedo, D. G. Jones, A. V. Jog, B. Jamshidi, D. R. Myers, L. Chen, X. Fu, M. Mehregany, M. B. J. Wijesundara, and A. P. Pisano, IEEE Sens. J. **7**, 568 (2007).

[4]D. G. Senesky, B. Jamshidi, K. B. Cheng, and A. P. Pisano, IEEE Sens. J. **9**, 1472 (2009).

[5]H.-P. Phan, T. Dinh, T. Kozeki, A. Qamar, T. Namazu, S. Dimitrijev, N.-T. Nguyen, and D. V. Dao, Sci. Rep. **6**, 28499 (2016).

[6]T. Nagai and M. Itoh, IEEE Trans. Ind. Appl. **26**, 1139 (1990).

[7]A. De Luca, G. Longobardi, and F. Udrea, in *Proceedings of 2015 International Semiconductor Conference (CAS), Sinaia, Romania* (IEEE, 2015), pp. 12–14.

[8]M. I. Lei, "Silicon carbide high temperature thermoelectric flow sensor," Ph.D thesis, Case Western Reserve University, 2011.

[9]R. N. Dean, G. T. Flowers, A. S. Hodel, G. Roth, S. Castro, R. Zhou, A. Moreira, A. Ahmed, R. Rifki, and B. E. Grantham, in 2007 *IEEE International Symposium on Industrial Electronics ISIE* (IEEE, 2007), pp. 1435–1440.

[10]A. R. Atwell, R. S. Okojie, K. T. Kornegay, S. L. Roberson, and A. Beliveau, Sens. Actuators, A **104**, 11 (2003).

[11]S. J. Mihailov, Sensors **12**, 1898 (2012).

[12]Y. Zhang, G. R. Pickrell, B. Qi, A. Safaai-Jazi, and A. Wang, Opt. Eng. **43**, 157 (2004).

[13]M. Kraft and N. M. White, *MEMS for Automotive and Aerospace Applications* (Woodhead Publishing Limited, Cambridge, 2013).

[14]A. N. Sinclair and A. M. Chertov, Ultrasonics **57**, 1 (2015).

[15]A. Baba, C. T. Searfass, and B. R. Tittmann, Appl. Phys. Lett. **97**, 232901 (2010).

[16]M. F. Haider, V. Giurgiutiu, B. Lin, and L. Yu, Smart Mater. Struct. **26**, 095019 (2017).

[17]P. Fürjes, G. Légrádi, C. Dücső, A. Aszódi, and I. Bársony, Sens. Actuators, A **115**, 417 (2004).

[18]A. Vescan, I. Daumiller, P. Gluche, W. Ebert, and E. Kohn, IEEE Electron Device Lett. **18**, 556 (1997).

[19]U. Schmid, Sens. Actuators, A **97**, 253 (2002).

[20]T. Moazzeni, J. Ma, Y. Jiang, and N. Li, IEEE Trans. Instrum. Meas. **60**, 2062 (2011).

[21]V. Lekholm, A. Persson, K. Palmer, F. Ericson, and G. Thornell, J. Micromech. Microeng. **23**, 055004 (2013).

[22]E. Vereshchagina, R. A. M. Wolters, and J. G. E. Gardeniers, Sens. Actuators, A **169**, 308 (2011).

[23]C. Sosna, M. Kropp, W. Lang, and R. Buchner, in *IEEE Sensors, 2010* (IEEE, 2010), pp. 2460–2463.

[24]M. Wijesundara and R. Azevedo, *Silicon Carbide Microsystems for Harsh Environments* (Springer Science & Business Media, 2011).

[25]R. Neul, U.-M. Gómez, K. Kehr, W. Bauer, J. Classen, C. Doring, E. Esch, S. Gotz, J. Hauer, and B. Kuhlmann, IEEE Sens. J. **7**, 302 (2007).

[26]B. Vivekananathan, L. Ponnusamy, and K. Thiruppathi, in 2015 *International Conference on Robotics, Automation, Control and Embedded Systems (RACE)* (IEEE, 2015), pp. 1–5.

[27]K. Thiruppathi, L. Ponnusamy, and B. Vivekananathan, in 2015 *International Conference on Robotics, Automation, Control and Embedded Systems (RACE)* (IEEE, 2015), pp. 1–6.

[28]W. J. Fleming, IEEE Sens. J. **1**, 296 (2001).

[29]R. A. Furness, *Fluid Flow Measurement* (Longman, London, UK, 1989).

[30]Y. Zhao, K. Chen, and J. Yang, Measurement **38**, 230 (2005).

[31]R. C. Baker, *Flow Measurement Handbook: Industrial Designs, Operating Principles, Performance, and Applications* (Cambridge University Press, 2005).

[32]G. C. Fralick, J. D. Wrbanek, and D. P. Hwang, "Thin-film air-mass-flow sensor of improved design developed," Technical Report 20050214769, Publication Information: Research and Technology 2002, NASA/TM-2003-211990, 2003, available at https://ntrs.nasa.gov/search.jsp?.

[33]C. Lyons, A. Friedberger, W. Welser, G. Muller, G. Krotz, and R. Kassing, in *Proceedings of Eleventh Annual International Workshop on Micro Electro Mechanical Systems 1998. MEMS 98* (IEEE, 1998), pp. 356–360.

[34]N. T. Nguyen, Flow Meas. Instrum. **8**, 7 (1997).

[35]J. Hong, Y. S. Chang, and D. Kim, Meas. Sci. Technol. **21**, 105408 (2010).

[36]R. Ahrens and M. Festa, J. Micromech. Microeng. **20**, 064004 (2010).

[37]R. Buchner, C. Sosna, M. Maiwald, W. Benecke, and W. Lang, Sens. Actuators, A **130–131**, 262 (2006).

[38]J. Wu and W. Sansen, Sens. Actuators, A **97–98**, 68–74 (2002).

[39]M. Ritterath, P. Voser, W. Dietze, H.-M. Prasser, and D. Paladino, in *IEEE Sensors, 2009* (IEEE, 2009), pp. 1419–1422.

[40]J. T. W. Kuo, L. Yu, and E. Meng, Micromachines **3**, 550 (2012).

[41]V. Balakrishnan, H.-P. Phan, T. Dinh, D. V. Dao, and N.-T. Nguyen, Sensors **17**, 2061 (2017).

[42]J. Chen, Z. Fan, J. Zou, J. Engel, and C. Liu, J. Aerosp. Eng. **16**, 85 (2003).

[43]S. C. C. Bailey, G. J. Kunkel, M. Hultmark, M. Vallikivi, J. P. Hill, K. A. Meyer, C. Tsay, C. B. Arnold, and A. J. Smits, J. Fluid Mech. **663**, 160 (2010).
[44]R. J. Adamec and D. V. Thiel, IEEE Sens. J. **10**, 847 (2010).
[45]S.-T. Hung, S.-C. Wong, and W. Fang, Sens. Actuators, A **84**, 70 (2000).
[46]C. Liu, J.-B. Huang, Z. A. Zhu, F. Jiang, S. Tung, Y.-C. Tai, and C.-M. Ho, J. Microelectromech. Syst. **8**, 90 (1999).
[47]P. Liu, R. Zhu, and R. Que, Sensors **9**, 9533 (2009).
[48]R.-H. Ma, D.-A. Wang, T.-H. Hsueh, and C.-Y. Lee, Sensors **9**, 5460 (2009).
[49]G. P. Shen, M. Qin, Q. A. Huang, H. Zhang, and J. Wu, Microsyst. Technol. **16**, 511 (2010).
[50]N. Therdthai, W. Zhou, and T. Adamczak, J. Food Eng. **63**, 329 (2004).
[51]Y. H. Wang, C. Y. Lee, and C. M. Chiang, Sensors **7**, 2389 (2007).
[52]Z. Fan, J. M. Engel, J. Chen, and C. Liu, J. Microelectromech. Syst. **13**, 484 (2004).
[53]F. Warkusz, J. Phys. D: Appl. Phys. **11**, 2035 (1978).
[54]B. W. van Oudheusden, Sens. Actuators, A **30**, 5 (1992).
[55]A. S. Cubukcu, E. Zernickel, U. Buerklin, and G. A. Urban, Sens. Actuators, A **163**, 449 (2010).
[56]P. Bruschi, M. Dei, and M. Piotto, IEEE Sens. J. **9**, 1688 (2009).
[57]G. Soundararajan, M. Rouhanizadeh, H. Yu, L. DeMaio, E. S. Kim, and T. K. Hsiai, Sens. Actuators, A **118**, 25 (2005).
[58]T. Dinh, H.-P. Phan, T.-K. Nguyen, A. Qamar, P. Woodfield, Y. Zhu, N.-T. Nguyen, and D. V. Dao, J. Phys. D: Appl. Phys. **50**, 215401 (2017).
[59]T. Dinh, H.-P. Phan, T.-K. Nguyen, A. Qamar, A. R. M. Foisal, T. N. Viet, C.-D. Tran, Y. Zhu, N.-T. Nguyen, and D. V. Dao, J. Mater. Chem. C **4**, 10061 (2016).
[60]J. Y. W. Seto, J. Appl. Phys. **46**, 5247 (1975).
[61]S.-G. Hur, D.-J. Kim, B.-D. Kang, and S.-G. Yoon, J. Vac. Sci. Technol., B: Nanotechnol. Microelectron.: Mater., Process., Meas., Phenom. **22**, 2698 (2004).
[62]H. P. Phan, T. Dinh, T. Kozeki, T. K. Nguyen, A. Qamar, T. Namazu, N. T. Nguyen, and D. V. Dao, Appl. Phys. Lett. **109**, 123502 (2016).
[63]N. Marsi, B. Y. Majlis, A. A. Hamzah, and F. Mohd-Yasin, Microsyst. Technol. **21**, 319 (2015).
[64]A. Harley-Trochimczyk, A. Rao, H. Long, A. Zettl, C. Carraro, and R. Maboudian, J. Micromech. Microeng. **27**, 045003 (2017).
[65]T. Dinh, H.-P. Phan, T.-K. Nguyen, V. Balakrishnan, H.-H. Cheng, L. Hold, A. Lacopi, N.-T. Nguyen, and D. V. Dao, IEEE Electron Device Lett. **39**, 580 (2018).
[66]V. Balakrishnan, T. Dinh, H.-P. Phan, D. V. Dao, and N.-T. Nguyen, Sens. Actuators, A **279**, 293 (2018).
[67]T. Dinh, H. Phan, A. Qamar, P. Woodfield, N. Nguyen, and D. V. Dao, J. Microelectromech. Syst. **26**, 966 (2017).
[68]T. Dinh, H.-P. Phan, D. V. Dao, P. Woodfield, A. Qamar, and N.-T. Nguyen, J. Mater. Chem. C **3**, 8776 (2015).
[69]F. Warkusz, J. Phys. D: Appl. Phys. **11**, 689 (1978).
[70]J. S. Shor, D. Goldstein, and A. D. Kurtz, IEEE Trans. Electron Devices **40**, 1093 (1993).
[71]T. Dinh, H.-P. Phan, T. Kozeki, A. Qamar, T. Namazu, N.-T. Nguyen, and D. V. Dao, RSC Adv. **5**, 106083 (2015).
[72]V. Balakrishnan, T. Dinh, H.-P. Phan, D. V. Dao, and N.-T. Nguyen, J. Heat Transfer **140**, 072001 (2018).
[73]V. Balakrishnan, T. Dinh, H.-P. Phan, T. Kozeki, T. Namazu, D. V. Dao, and N.-T. Nguyen, J. Micromech. Microeng. **27**, 075008 (2017).
[74]T. Dinh, H.-P. Phan, T. Kozeki, A. Qamar, T. Fujii, T. Namazu, N.-T. Nguyen, and D. V. Dao, Mater. Lett. **177**, 80 (2016).
[75]A. Bosseboeuf, P. E. Allain, F. Parrain, X. Le Roux, N. Isac, S. Jacob, A. Poizat, P. Coste, S. Maaroufi, and A. Walther, Adv. Nat. Sci.: Nanosci. Nanotechnol. **6**, 025001 (2015).
[76]C.-P. Wang, C.-W. Liu, and C. Gau, in *2011 IEEE International Conference on Nano/Micro Engineered and Molecular Systems (NEMS)* (IEEE, 2011), pp. 630–633.